Counterion Density Profiles at Charged Flexible Membranes

Christian C. Fleck[1] and Roland R. Netz[2]

[1]*Freiburg Ctr. for Data Analysis and Modeling, Albert-Ludwig University of Freiburg, Herman-Herder Strasse 3 79104 Freiburg, Germany*

[2]*Physik Department, Technische Universität Munich, James Franck Strasse, 85748 Garching, Germany*

(Received 17 September 2004; published 14 September 2005)

Counterion distributions at charged flexible membranes are studied using analytical and simulation methods in both Poisson-Boltzmann and strong-coupling limits. The softer the membrane, the more smeared out the counterion-density profile becomes and counterions penetrate through the mean-membrane surface location, in agreement with anomalous scattering results. Repulsion between membrane charges enhances protrusions and induces short-scale membrane roughening.

DOI: 10.1103/PhysRevLett.95.128101 PACS numbers: 87.16.Ac, 87.16.Dg, 87.68.+z

The study of charged colloids and biopolymers faces a fundamental problem: In theoretical investigations, the central object which is primarily computed is the charge density distribution in the electrolyte solution adjacent to the charged body [1]. Experimentally measurable observables are typically derived from this charge distribution. For example, the force between charged particles follows from the ion density at the particle surfaces via the contact-value theorem. Likewise, the surface tension and surface potential are obtained as weighted integrals over the ion distributions. It has proven difficult to measure the counterion distribution at a charged surface directly because of the small scattering intensity. Notable exceptions are neutron scattering contrast variation with deuterated and protonated organic counterions [2] and local fluorescence studies on Zinc-ion distributions using x-ray standing waves [3]. Clearly, direct comparisons between theoretical and experimental ion distributions (rather than derived quantities) is desirable as it provides important hints how to improve theoretical modeling.

In a landmark paper the problem of low intensity was overcome by anomalous x-ray scattering on stacks of highly charged bilayer membranes [4], allowing us to sensitively discriminate counterion scattering from the background. Since then, similar techniques have been applied to charged biopolymers [5,6] and to oriented charged bilayer stacks, where the problem of powder averaging is avoided [7]. However, scattering on soft biomaterials brings in a new complication, not considered theoretically so far: soft membranes and biopolymers fluctuate in shape, and thus perturb the counterion-density profile. Comparison with standard theories for rigid charged objects of simple geometric shape becomes impossible. Here we fill this gap by considering the counterion-density profile close to a planar charged membrane which exhibits shape fluctuations governed by bending rigidity.

We derive for a relatively stiff membrane closed form expressions for the counterion-density profile; they depend crucially on the membrane stiffness and are quite different in the asymptotic low and high-charge limits. The analytic density profiles, which compare favorably with our simulation results, will facilitate the analysis of scattering data since they allow for fits with few physical parameters. In previous experiments, a puzzling ion penetration into the lipid region was detected but interpreted as an artifact [4]. We show that ion penetration indeed occurs and is due to correlated ion-membrane fluctuations. The electrostatic repulsion between membrane charges also renormalizes the membrane elasticity: since membrane protrusion modes are electrostatically favored, the short-scale bending rigidity is reduced and the membranes become locally rougher.

The Hamiltonian $H = H_m + H_e$ of the membrane-counterion system consists of the elastic membrane part H_m, and the electrostatic part H_e. We discretize the membrane shape on a two-dimensional $N_L \times N_L$ square lattice with lattice constant a and rescale all lengths by the Gouy-Chapman length $\mu = 1/2\pi q \ell_B \sigma_m$ according to $\mathbf{r} = \mu\tilde{\mathbf{r}}$, where $\sigma_m = QM/N_L^2 a^2$ is the projected charge density of the membrane and $\ell_B = e^2/4\pi\varepsilon_0\varepsilon k_B T$ is the Bjerrum length (e is the elementary charge, ε the dielectric constant). Parametrizing the membrane shape by the height function $h(\mathbf{x})$, the elastic membrane energy in harmonic approximation reads in units of $k_B T$ [8]

$$H_m[\tilde{h}] = \frac{K_0}{2}\int d^2\tilde{x}[\Delta\tilde{h}(\tilde{\mathbf{x}})]^2 + \frac{\tilde{g}}{2}\int d^2\tilde{x}\tilde{h}^2(\tilde{\mathbf{x}}), \quad (1)$$

where Δ is the Laplace operator, K_0 is the bare bending rigidity and $\tilde{g} = g\mu^4$ is the rescaled strength of the harmonic potential. The electrostatic energy accounts for the interaction of N counterions of valence q and M membrane charges of valence Q, related by the electroneutrality condition $QM = qN$,

$$H_e = \sum_{i=1}^{N-1}\sum_{j=i+1}^{N}\frac{\Xi}{|\tilde{\mathbf{r}}_i - \tilde{\mathbf{r}}_j|} - \sum_{i=1}^{N}\sum_{k=1}^{M}\frac{Q/q\Xi}{|\tilde{\mathbf{r}}_i - \tilde{\mathbf{R}}_k|} + \sum_{k}^{M-1}\sum_{l=k+1}^{M}\frac{(Q/q)^2\Xi}{|\tilde{\mathbf{R}}_k - \tilde{\mathbf{R}}_l|} \quad (2)$$

where $\Xi = 2\pi q^3 \ell_B^2 \sigma_m$ denotes the coupling parameter [9]. The position of the ith counterion is $\tilde{\mathbf{r}}_i$ while the kth membrane ion is located at $\tilde{\mathbf{R}}_k = (\tilde{\mathbf{x}}_k, \tilde{h}(\tilde{\mathbf{x}}_k) - \tilde{d})$ and dis-

placed by $\tilde{d} = 2\tilde{a}N_L M^{-1/2}$ beneath the membrane surface which is impenetrable to the pointlike counterions. With this value of $\tilde{d}$ we can neglect charge-discreteness effects [10] and concentrate on membrane-shape–fluctuation effects. In most of our simulations the membrane ions are mobile and move freely on the membrane lattice, with a packing fraction $\zeta = M/N_L^2$. For the long-ranged electrostatic interactions we employ laterally periodic boundary conditions using Lekner-Sperb methods [9]. Simulations are run for typically 10^6 Monte Carlo steps using 100 counterions and 100 membrane ions. In Fig. 1 we show two simulation snapshots. The counterions form in the weak-coupling limit [$\Xi = 0.2$, Fig. 1(a)] a diffuse dense cloud while in the strong-coupling limit [$\Xi = 1000$, Fig. 1(b), note the anisotropic rescaling] the lateral ion-ion distances are large compared to the mean separation from the membrane. Pronounced correlations between membrane shape fluctuations and counterion positions are observed in both snapshots.

The qualitatively different ionic structures at low/high coupling strength are reflected by fundamentally different analytic approaches in these two limits: the starting point is the exact field-theoretic formulation of the partition function of the system [11]

$$\mathcal{Z} \simeq \int \mathcal{D}\tilde{h}\mathcal{D}\phi e^{-H_m[\tilde{h}]-H_\phi[\tilde{h},\phi]/\Xi}. \tag{3}$$

The field $i\phi$ is the fluctuating electrostatic potential [11]. The electrostatic action reads

$$H_\phi[\tilde{h},\phi] = \frac{1}{8\pi}\int d\tilde{\mathbf{r}}[\nabla\phi(\tilde{\mathbf{r}})]^2 - \frac{i}{2\pi}\int d\tilde{\mathbf{r}}\delta(\tilde{z}-\tilde{h}(\tilde{\mathbf{x}}))\phi(\tilde{\mathbf{r}}) - \frac{\Lambda}{2\pi}\int d\tilde{\mathbf{r}}e^{-i\phi(\tilde{\mathbf{r}})}\theta(\tilde{z}-\tilde{h}(\tilde{\mathbf{x}})) \tag{4}$$

where $\theta(z) = 1$ for $z > 0$ and zero otherwise. The expectation value of the counterion density reads

$$\bar{\rho}(\tilde{\mathbf{r}}) = \frac{\rho(\tilde{\mathbf{r}})}{2\pi\ell_B\sigma_m^2} = \Lambda\langle\theta(\tilde{z}-\tilde{h}(\tilde{\mathbf{x}}))e^{-i\phi(\tilde{\mathbf{r}})}\rangle. \tag{5}$$

The dimensionless fugacity Λ is determined by the normalization condition $\int d\tilde{z}\,\bar{\rho}(\tilde{z}) = 1$. In the weak-coupling limit, $\Xi \to 0$, fluctuations of the field ϕ around the saddle point value are small and Gaussian variational methods become accurate. The variational Gibbs free energy reads $F_v = F_0 + \langle H_\phi[\tilde{h},\phi]/\Xi + H_m[\tilde{h}] - H_0[\tilde{h},\phi]\rangle_0$, where $\langle\ldots\rangle_0$ is an average with the variational Hamiltonian H_0 and F_0 is the corresponding free energy. The most general Gaussian variational Hamiltonian is $2H_0[\tilde{h},\phi] = \int d\tilde{\mathbf{x}}d\tilde{\mathbf{x}}'\tilde{h}(\tilde{\mathbf{x}})K^{-1}(\tilde{\mathbf{x}},\tilde{\mathbf{x}}')\tilde{h}(\tilde{\mathbf{x}}') + \int d\tilde{\mathbf{r}}d\tilde{\mathbf{r}}'\Omega(\tilde{\mathbf{r}})v^{-1}(\tilde{\mathbf{r}},\tilde{\mathbf{r}}')\Omega(\tilde{\mathbf{r}}')$, where the field Ω is defined by $\Omega(\tilde{\mathbf{r}}) := \phi(\tilde{\mathbf{r}}) - \phi_0(\tilde{\mathbf{r}}) + i\int d\tilde{\mathbf{x}}'d\tilde{\mathbf{x}}''P(\tilde{\mathbf{r}};\tilde{\mathbf{x}}')K^{-1}(\tilde{\mathbf{x}}',\tilde{\mathbf{x}}'')\tilde{h}(\tilde{\mathbf{x}}'')$; and P is the connected correlation function $P(\tilde{\mathbf{r}};\tilde{\mathbf{x}}') = \langle i\phi(\tilde{\mathbf{r}})\tilde{h}(\tilde{\mathbf{x}}')\rangle_0^c$. The variational parameters are the mean potential ϕ_0, the coupling operator P, the propagator of the electrostatic field v, and the membrane propagator K. For K we use the bare propagator of the uncharged membrane [8], giving a bare membrane roughness of $(\tilde{\xi}_\perp^0)^2 := \langle\tilde{h}^2(0)\rangle_0 = 1/\sqrt{64K_0\tilde{g}}$. Assuming the charge propagator v to be isotropic and translational invariant (which is an approximation), v turns out to be the bare Coulomb propagator, $v(\mathbf{r}) = 1/r$. The remaining variational equations $\delta F_v/\delta P = \delta F_v/\delta\phi_0 = 0$ are solved perturbatively in an asymptotic small $\tilde{\xi}_\perp^0$ expansion, i.e., for a relatively stiff membrane. The solution for P for $\tilde{\mathbf{x}} = \tilde{\mathbf{x}}'$ is expressed in terms of the Meijer's $\mathcal{G}$ function and reads [neglecting terms of $\mathcal{O}((\tilde{\xi}_\perp^0)^3)$]: $P_\perp(\tilde{z}) = -[(\tilde{\xi}_\perp^0)^2/\sqrt{2\pi^5}]\,\mathrm{erf}[\tilde{z}/\sqrt{2(\tilde{\xi}_\perp^0)^2}] \times \mathcal{G}_{1,5}^{5,1}[(\tilde{z}/64\tilde{\xi}_\parallel^0)^4|\{\frac{1}{2}\},\{0,\frac{1}{4},\frac{1}{2},\frac{1}{2},\frac{3}{4}\}]$. The result for the mean potential ϕ_0 is shown in Eq. (6) and reduces in the limit $\tilde{\xi}_\perp^0 \to 0$ to the known Gouy-Chapmann potential $i\phi(\tilde{z}) = 2\ln(1+\tilde{z})$ [9]. We defined the auxiliary function $w(\tilde{z})$ as $w(\tilde{z}) := \sqrt{2(\tilde{\xi}_\perp^0)^2/\pi}\exp\{-\tilde{z}^2/2(\tilde{\xi}_\perp^0)^2\} - \tilde{z}\,\mathrm{erfc}[\tilde{z}/\sqrt{2(\tilde{\xi}_\perp^0)^2}]$. The counterion density according to Eq. (5) is given by Eq. (7); it reduces to the known mean-field counterion density $\bar{\rho}_{\mathrm{PB}}(\tilde{z}) = (1+\tilde{z})^{-2}$ in the case of vanishing membrane roughness $\tilde{\xi}_\perp^0$ [9,12]. In Fig. 2 we show the laterally averaged counterion-density profiles for weak coupling $\Xi = 0.2$ obtained from Monte Carlo (MC) simulation (solid squares) for several membrane roughnesses. For the comparison with the analytical expression Eq. (7) (solid lines) we use the discrete membrane

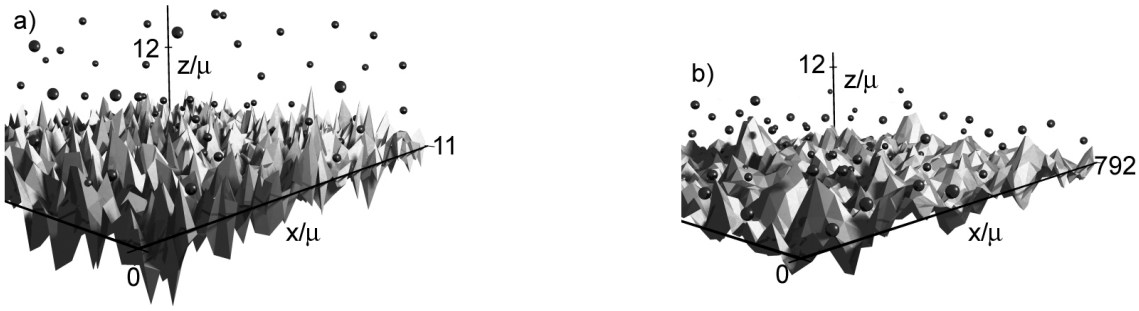

FIG. 1. Snapshots for (a) weak coupling $\Xi = 0.2$, $\xi_\perp^0/\mu = 0.80$, $K_0 = 0.07$, $\tilde{g} = 0.57$, $\tilde{a} = 0.18$ and (b) strong coupling $\Xi = 1000$, $\xi_\perp^0/\mu = 0.38$, $K_0 = 174$, $\tilde{g} = 0.006$, $\tilde{a} = 13.21$. Simulations are done with $N = 100$ counterions and $M = 100$ membrane ions on a $N_L^2 = 60 \times 60$ membrane lattice.

propagator $K_{mn}^{-1} = 4K_0(\cos[2\pi n/N_L] + \cos[2\pi m/N_L] - 2)^2/\tilde{a}^4 + \tilde{g}$ and calculate the membrane roughness according to $(\tilde{\xi}_\perp^d)^2 = (2\pi/\tilde{a}N_L)^2 \sum_{m,n} K_{mn}$, the lateral correlation length follows as $\tilde{\xi}_\parallel^d = 1/(2\tilde{\xi}_\perp^d \tilde{g}^{1/2})$. For the comparison in Fig. 2 we insert $\tilde{\xi}_\perp^d$ into Eq. (7). The general agreement is very good, for the roughest membrane with $\tilde{\xi}_\perp^d = 1.211$ some deviations are observed, signaling the breakdown of our small $\tilde{\xi}_\perp^0$ expansion.

$$i\phi_0(\tilde{z}) = \left\{ \begin{array}{c} w(\tilde{z}) + 2\ln[1 + \tilde{z} - \tilde{z}w(\tilde{z})/4 - (\tilde{\xi}_\perp^0/2)^2 \operatorname{erf}(\frac{\tilde{z}}{\sqrt{2}\tilde{\xi}_\perp^0})] + \mathcal{O}((\tilde{\xi}_\perp^0)^3) : \tilde{z} \geq 0 \\ 2\tilde{z} - \tilde{z}^2 + w(\tilde{z})(1 - \tilde{z}/2) - (\tilde{\xi}_\perp^0)^2 \operatorname{erf}[\frac{\tilde{z}}{\sqrt{2}\tilde{\xi}_\perp^0}]/2 + \mathcal{O}((\tilde{\xi}_\perp^0)^3) : \tilde{z} < 0 \end{array} \right\} \tag{6}$$

$$\bar{\rho}(\tilde{z}) = \frac{e^{-i\phi_0(\tilde{z})}}{2} \left\{ \left(1 + \operatorname{erf}\left[\frac{\tilde{z}}{\sqrt{2}\tilde{\xi}_\perp^0}\right]\right)\left(1 - \frac{P_\perp(\tilde{z})}{2} \operatorname{erf}\left[\frac{\tilde{z}}{\sqrt{2}\tilde{\xi}_\perp^0}\right]\right) + 2P_\perp(\tilde{z}) \frac{e^{-(\tilde{z}/\tilde{\xi}_\perp^0)^2/2}}{\sqrt{2\pi}\tilde{\xi}_\perp^0} \right\} + \mathcal{O}((\tilde{\xi}_\perp^0)^3). \tag{7}$$

In the strong-coupling limit $\Xi \to \infty$, we expand the partition function equation (3) in inverse powers of Ξ [9]. We find for the leading term of the density equation (5)

$$\bar{\rho}(\tilde{\mathbf{r}}) = \frac{\Lambda}{Z} \int \mathcal{D}\tilde{h}\theta(\tilde{z} - \tilde{h}(\tilde{\mathbf{x}}))e^{-H_m[\tilde{h}] - V[\tilde{h}]} + \mathcal{O}\left(\frac{1}{\Xi}\right). \tag{8}$$

The interaction term V is given by $V[\tilde{h}] = -\tilde{z} + \int d\tilde{\mathbf{r}}' \tilde{h}(\tilde{\mathbf{x}}') f_{\tilde{h}}(\tilde{\mathbf{r}}, \tilde{\mathbf{r}}')$, with the function $f_{\tilde{h}}$, defined by $f_{\tilde{h}}(\tilde{\mathbf{r}}, \tilde{\mathbf{r}}') := \delta(\tilde{z}' - \tilde{h}(\tilde{\mathbf{x}}'))[(\tilde{z} - \tilde{z}') - (\tilde{\mathbf{x}} - \tilde{\mathbf{x}}') \cdot \nabla' \tilde{h}(\tilde{\mathbf{x}}')]/2\pi[|\tilde{\mathbf{x}} - \tilde{\mathbf{x}}'|^2 + (\tilde{z} - \tilde{z}')^2]^{3/2}$. To calculate the integral equation (8) we expand in powers of $f_{\tilde{h}}$, which gives rise to

$$\bar{\rho}(\tilde{z}) = \frac{e^{-\tilde{z} - (\tilde{\xi}_\perp^0)^2/2}}{2} \left(1 + \operatorname{erf}\left[\frac{\tilde{z}}{\sqrt{2}\tilde{\xi}_\perp^0}\right]\right) + \mathcal{O}\left(\frac{1}{\Xi}, f_{\tilde{h}}\right). \tag{9}$$

The density (9) reduces to the known strong-coupling density $\bar{\rho}_{\mathrm{SC}}(\tilde{z}) = e^{-\tilde{z}}$ in the limit $\tilde{\xi}_\perp^0 \to 0$ [9]. We compare in Fig. 2 the analytically obtained counterion-density profiles (solid lines) with the laterally averaged densities obtained using MC simulations (open triangles) for $\Xi = 1000$ and different $\tilde{\xi}_\perp^d$. The analytic approximation reproduces the simulated profiles very well. Comparison of mobile and immobile membrane ions gives no detectable difference for the counterion profile, also the membrane-ion fraction ζ plays a minor role (Fig. 2 inset). As can be seen in Fig. 2, the counterion profiles are noticeably different in the low and large-coupling regimes, an effect well captured by the analytic expressions equations (7) and (9). The membrane roughness $\xi_\perp$ as well as the coupling parameter Ξ can be varied experimentally by changing the membrane composition, e.g., the ratio of charged to uncharged lipids, the valence of the counterions, the amount of cholesterol, etc. Neglecting the correlations between membrane and counterion fluctuations results for small coupling in the expression $\bar{\rho}(\tilde{z}) = \int d\tilde{h} w(\tilde{h}) \bar{\rho}_{\mathrm{PB}}(\tilde{z} - \tilde{h})$, where $w(\tilde{h}) = e^{-(\tilde{h}/\tilde{\xi}_\perp^0)^2/2}/\sqrt{2\pi}\tilde{\xi}_\perp^0$ is the normalized membrane height distribution (with a similar expression using $\bar{\rho}_{\mathrm{SC}}$ in the strong-coupling limit). Such a factorization approximation never works well, and in specific does not reproduce the fact that the maximum of the counterion-density distribution is located at negative values of $\tilde{z}$ for strong coupling (see Fig. 2).

In the analytics so far we used the bare membrane roughness $\tilde{\xi}_\perp^d$ without modification due to electrostatics. In Fig. 3 we show the ratio of $\tilde{\xi}_\perp = (\langle \tilde{h}^2(0) \rangle)^{1/2}$, the membrane roughness measured in the MC simulation, and $\tilde{\xi}_\perp^d$, for the bare uncharged membrane, as a function of the coupling parameter Ξ for two different membrane-ion fractions ζ (open symbols). The ratio is larger than unity, i.e., charges on the membrane enhance protrusions which increase their mutual distance [13]. Experimentally, protrusions are created by vertical shifts of single lipids. Since protrusions, which form the local degrees of freedom in our simulations (and are also included in the analytic theory since we keep the projected area constant), do not conserve the true membrane area, the roughening we discuss here has to be distinguished from the electrostatic stiffening in

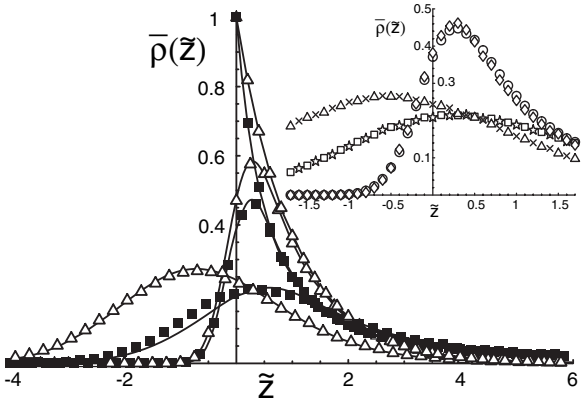

FIG. 2. Rescaled counterion density $\bar{\rho}(\tilde{z}) = \rho(\tilde{z})/2\pi\ell_B\sigma_m^2$ as a function of the rescaled distance $\tilde{z} = z/\mu$ from Monte Carlo simulations (data points) and asymptotic theory [solid lines, Eqs. (7) and (9)]. In the weak-coupling limit ($\Xi = 0.2$, solid squares), the membrane roughness is $\tilde{\xi}_\perp^d = 1.211, 0.3184, 0$ and $\tilde{\xi}_\parallel^d = 0.2483, 0.2933, \infty$ from bottom to top. In the strong-coupling limit ($\Xi = 1000$, open triangles) we have $\tilde{\xi}_\perp^d = 1.211, 0.3184, 0$ and $\tilde{\xi}_\parallel^d = 17.2475, 20.7458, \infty$ from bottom to top. Numerical errors are smaller then the symbol sizes. In all cases the membrane ions are mobile and the packing fraction is $\zeta = 0.028$. The inset compares profiles for $\Xi = 0.2$, $\tilde{\xi}_\perp^d = 0.3184$ for $\zeta = 0.028$ (diamonds) and $\zeta = 0.25$ (circles) for mobile membrane ions and results for $\Xi = 0.2$, $\tilde{\xi}_\perp^d = 1.211$, $\zeta = 0.028$ for mobile (squares) and fixed (stars) membrane ions and $\Xi = 1000$, $\tilde{\xi}_\perp^d = 1.211$, $\zeta = 0.028$ for mobile (triangle) and fixed (crosses) membrane ions.

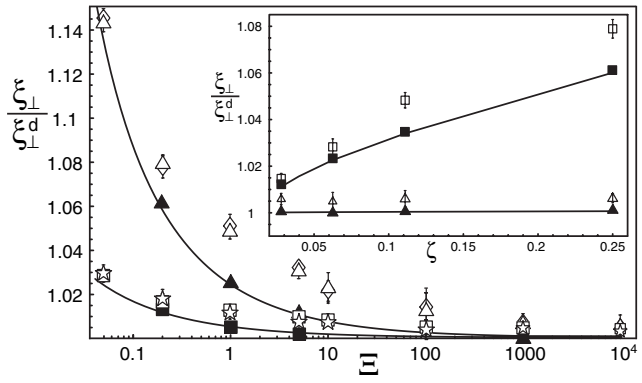

FIG. 3. Ratio of simulated and bare roughness $\tilde{\xi}_\perp/\tilde{\xi}_\perp^d$ as a function of coupling strength Ξ for membrane-ion fraction $\zeta = 0.028$ and membrane roughness $\tilde{\xi}_\perp^d = 0.3184$ (open squares) and $\tilde{\xi}_\perp^d = 1.2111$ (open stars), $\zeta = 0.25$ and $\tilde{\xi}_\perp^d = 0.3184$ (open triangles) and $\tilde{\xi}_\perp^d = 1.2111$ (open diamonds). The solid lines and solid symbols are analytical and MC results without counterions ($\zeta = 0.028$ lower branch, $\zeta = 0.25$ upper branch). The inset shows the ratio $\tilde{\xi}_\perp/\tilde{\xi}_\perp^d$ as a function of ζ for $\Xi = 0.2$ (open squares) and $\Xi = 1000$ (open triangles), $\tilde{\xi}_\perp^d = 0.3184$ in both cases. The solid lines and solid symbols are analytical and MC results without counterions ($\Xi = 1000$ lower branch, $\Xi = 0.2$ upper branch).

the long-wavelength limit as predicted on the mean-field level for single membranes [14–16] and for multimembrane systems [17]. Conversely, in the strong-coupling limit, electrostatic correlations effects tend to decrease the bending rigidity with a pronounced wavelength dependence [18–20]. Experimentally, both membrane stiffening [21] and, for highly charged membranes, softening has been observed [22]. The membrane roughness results from a sum of the membrane propagator over the entire q-mode spectrum, $\tilde{\xi}_\perp^2 = (2\pi/\tilde{a}N_L)^2 \sum_{\tilde{q}} \langle \tilde{h}_{\tilde{q}}^2 \rangle$. Since the roughening is most pronounced for small coupling (see Fig. 3), we conclude that charged membranes that can form protrusions exhibit in the weak-coupling limit a scale-dependent rigidity that must be highly reduced for small length scales and thus overcompensates the large-scale stiffening.

To understand the membrane roughening better, we calculate via exact enumeration and within harmonic approximation the membrane roughness for a charged discrete membrane without counterions. The roughness ratio from this analytical calculation is shown in Fig. 3 by solid lines, and compared with MC simulations of the corresponding system without counterions (filled symbols). Perfect agreement between filled symbols and solid lines shows that the harmonic approximation is valid. Good agreement between solid lines and the MC data that include counterions (open symbols) further shows that the roughening effect is indeed due to the repulsion of charges on the membrane itself, and counterions play a minor role. Experimentally, this membrane roughening might be observable with diffuse x-ray scattering; since it is due to a membrane softening at short length scales, it will also be present at finite ionic strength, as long as the average distance between membrane ions is smaller than the bulk screening length.

Financial support by the ''International Research Training Group Soft Condensed Matter'' at the University of Konstanz, Germany, is acknowledged.

[1] *Electrostatic Effects in Soft Matter and Biophysics*, edited by C. Holm, P. Kekicheff, and R. Podgornik (Kluwer Academic Publishers, Dordrecht, 2001).
[2] M. P Hentschel, M. Mischel, R. C. Oberthür, and G. Büldt, FEBS Lett. **193**, 236 (1985).
[3] J. Wang, M. Caffrey, M. J. Bedzyk, and T. L. Penner, Langmuir **17**, 3671 (2001).
[4] H. Richardsen, U. Vierl, G. Cevc, and W. Fenzl, Europhys. Lett. **34**, 543 (1996).
[5] R. Das *et al.*, Phys. Rev. Lett. **90**, 188103 (2003).
[6] T. E. Angelini, H. Liang, W. Wriggers, and G. C. L. Wong, Proc. Natl. Acad. Sci. U.S.A. **100**, 8634 (2003).
[7] G. Brotond and T. Salditt, Anal. Bioanal. Chem. **379**, 960 (2004).
[8] R. Lipowsky, in *The Structure and Dynamics of Membranes*, Handbook on Biological Physics Vol. 1 (Elsevier, Amsterdam, 1995).
[9] A. G. Moreira and R. R. Netz, Eur. Phys. J. E **8**, 33 (2002).
[10] A. G. Moreira and R. R. Netz, Europhys. Lett. **57**, 911 (2002); D. B. Lukatsky, S. A. Safran, A. W. C. Lau, and P. Pincus, *ibid.* **58**, 785 (2002); C. C. Fleck, R. R. Netz, *ibid.* **70**, 341 (2005).
[11] R. R. Netz and H. Orland, Eur. Phys. J. E **1**, 203 (2000).
[12] The final expression for the density equation (7) is considerably simplified but remains sufficiently accurate by setting $P_\perp = 0$.
[13] For membranes with a finite stretching modulus, electrostatics also modify the projected membrane area; see A. W. C. Lau and P. Pincus, Eur. Phys. J. B **10**, 175 (1999).
[14] M. Winterhalter and W. Helfrich, J. Phys. Chem. **92**, 6865 (1988).
[15] H. N. W. Lekkerkerker, Physica (Amsterdam) **159A**, 319 (1989).
[16] D. J. Mitchell and B. W. Ninham, Langmuir **5**, 1121 (1989).
[17] P. Pincus, J.-F. Joanny, and D. Andelman, Europhys. Lett. **11**, 763 (1990).
[18] A. W. C. Lau and P. Pincus, Phys. Rev. Lett. **81**, 1338 (1998).
[19] R. R. Netz, Phys. Rev. E **64**, 051401 (2001).
[20] Y. W. Kim and W. Sung, Europhys. Lett. **58**, 147 (2002).
[21] A. C. Rowat, P. L. Hansen, and J. H. Ipsen, Europhys. Lett. **67**, 144 (2004).
[22] B. Deme, M. Dubois, and T. Zemb, Langmuir **18**, 1005 (2002).